Welding in the World (2024) 68:117–136
https://doi.org/10.1007/s40194-023-01636-x

RESEARCH PAPER

Frontal pyrometric snapshot measurements of the keyhole wall temperature in laser welding of pure aluminium

R. Pordzik[1] · T. Mattulat[1] · P. Woizeschke[2]

Received: 24 August 2023 / Accepted: 11 November 2023 / Published online: 24 November 2023

Abstract
In deep penetration laser welding, the quality of the weld seam is strongly correlated with the process dynamics. Pronounced dynamics of the melt pool and the keyhole cause defects like pores and blow-outs which negatively affect the mechanical properties of the seam. The process dynamics are primarily governed by the fluctuations of the keyhole shape. Therefore, in order to avoid the occurrence of defects in the weld seam, it is necessary to gain control over the keyhole stability by understanding the underlying physical processes that contribute to its dynamics. Besides the intensity distribution of the laser beam on the keyhole walls, the keyhole wall temperature is a crucial influencing factor when it comes to the assessment of the local metal evaporation rate and the induced local recoil pressure acting on the keyhole wall. Using small high-melting tantalum probes as measuring channels, temperatures in the vicinity of the Knudsen layer at the keyhole front wall were measured at different depths below the sample surface by means of high-speed pyrometry. For this purpose, bead on plate welding was conducted at low process velocities in the Rosenthal regime using pure aluminium (EN AW-1050A) as substrate material. It is shown for different laser powers and process velocities that the melt temperature in the vicinity of the keyhole wall lies in the range of 3000 K ± 400 K, therefore intermittently exceeding the vaporisation temperature of the substrate material. Significant correlations between the keyhole wall temperature and the laser power as well as the measuring depth could not be identified.

Keywords Joining · Laser beam welding · Keyhole dynamics · Pyrometry · Aluminium alloys

1 Introduction

Deep penetration laser welding is a widely applied joining technique that allows fast and energy efficient welding of metals. The laser radiation melts and vaporises the substrate material in the region of direct laser material interaction. By surpassing a material specific intensity threshold, the recoil pressure of the vaporised material acting onto the substrate surface becomes sufficiently high to form a vapour capillary that is referred to as keyhole [1]. Thus, the keyhole is by nature nothing else but an indentation of the melt pool surface at the location of direct laser material interaction formed by the evaporation pressure of metal evaporating locally at high rates. The presence of the keyhole has a drastic impact on the absorption of the laser power into the substrate material by enabling multiple reflections of the laser beam on the keyhole walls [2], resulting in, for example, overall power absorptions of up to 93% at welding velocities below 6000 mm/min according to [3]. The resulting welds exhibit a high ratio between the depth and the width of the seam as well as a narrow heat affected zone. Despite these advantages, the keyhole is highly dynamic, resulting in strong fluctuations of its shape regarding the keyhole depth and the contour of the keyhole walls during the welding process [4]. Process defects like the formation of pores and blow-outs as a consequence of keyhole collapses

Recommended for publication by Commission IV—Power Beam Processes.

✉ R. Pordzik
pordzik@bias.de

T. Mattulat
mattulat@bias.de

P. Woizeschke
peer.woizeschke@tu-dortmund.de

[1] BIAS–Bremer Institut für angewandte Strahltechnik GmbH, Klagenfurter Straße 5, 28359 Bremen, Germany

[2] TU Dortmund University–Group LMP+ (Affiliated with ISF), Baroper Straße 303, 44227 Dortmund, Germany

and constrictions are commonly known to negatively affect the qualities of the weld seams [5].

Laser deep penetration welding is a process of high physical complexity as it emerges from the dynamic interplay of the welded material in its three states of aggregation. The solid state constitutes the mechanical boundary conditions for the melt pool dynamics as well as a thermal interface and sink for heat conduction. The liquid phase constitutes the melt pool enclosing the keyhole. The melt pool dynamics are primarily governed by the response of the molten material to external forces as well as to gradients in the temperature field and the local viscosity by convection, respectively. The flow dynamics in laser deep penetration welding was investigated by Matsunawa et al. who characterised flow patterns in the melt using X-ray recordings of the process in combination with tracer particles [6]. Simulative approaches to describe the melt pool dynamics were investigated, e.g. by Otto et al., by means of fluid-dynamical modelling of the laser deep penetration process [7]. The vapour phase constitutes the driving mechanical force acting on the melt pool surface leading to the formation of the keyhole. Inside the keyhole, the vapour is still exerting pressure onto the keyhole walls constituting a main opening force of the vapour capillary but also acting as a redistributor of energy, thus influencing the temperature distribution on the keyhole walls [8]. As the laser power is substantially absorbed at the keyhole front wall as well as at the keyhole bottom due to the progression of the keyhole in the welding direction [9], humps and steps at the keyhole front wall lead to increased local absorption and vapour jets directed towards the keyhole rear, destabilising the keyhole and ultimately leading to keyhole collapses and pore formation [10]. While the interface between the melt pool and the solid substrate material as well as the melt pool surface predominately dissipate heat into the surrounding material or atmosphere, the energy input alongside the driving mechanical forces happens inside the keyhole driven by laser absorption and material evaporation consequently. In order to characterise both, the local evaporation rate as a source of mechanical pressure on the keyhole walls as well as the local heat input influencing the temperature field of the melt pool and thereby the flow dynamics, the knowledge of locally absorbed laser intensity is required. The laser absorption inside the keyhole is essentially accomplished by two mechanisms, the first being Fresnel absorption at the interface between the vapour and liquid phase and the second being inverse Bremsstrahlung describing the intensity reduction of the laser beam when passing through a gaseous phase [11]. Fresnel absorption by its nature defines the local intensity absorption of the laser beam at the keyhole walls depending on the angle of incidence, the wavelength of the laser radiation and ultimately the temperature as well as the material composition of the absorbing surface itself. Thus, the Fresnel absorption is the driving mechanism for inducing the local material evaporation resulting in a locally dependent pressure field defined at the keyhole wall. For example, an analytical model introduced by Volpp demonstrated the influence of spatial power distribution of the laser beam inside the keyhole on the resulting keyhole geometry [12]. The thin layer at the keyhole front wall, where laser material interaction and evaporation occur, is called the Knudsen layer [13]. In this layer of only a few mean free path lengths in thickness, the velocity distribution relaxes from a highly non-equilibrium distribution on the liquid interface to a shifted Maxwell–Boltzmann distribution. Evidence has been presented for the overheating of melt in the vicinity of the Knudsen layer as predicted by the numeric model proposed by Ki et al. [14].

The strong interdependence between the local heat input, the keyhole shape and the melt flow around it leads to process dynamics that are a priori difficult to predict and most importantly hard to control. Therefore, in order to beneficially influence and stabilise the process behaviour, gaining insights into the complex and transient physical phenomena involved on a fundamental scale is inevitable. The keyhole constitutes a rather challenging measurement environment for most measuring techniques as temperatures above 2000 K, vaporous and electromagnetic process emissions and a difficult accessibility due to the high aspect ratios impede most conventional measuring techniques to probe the inside of the keyhole. Nonetheless, a few methods have been proven suitable for on-line measurements of the keyhole process such as optical coherence tomography (OCT), X-ray imaging and high-speed recordings through the keyhole opening. These measurement techniques allow for the time-resolved analysis of the keyhole shape as OCT yields the possibility of determining the keyhole depth [15], X-ray imaging yields the opportunity of recording the complete keyhole shape [16] and high-speed imaging was applied for monitoring the surface structure of the keyhole front wall [17]. The keyhole wall temperature as a crucial physical quantity for a detailed comprehension of the laser absorption and the local evaporation remains difficult to measure as measuring the temperatures directly through the keyhole opening is heavily impeded by scattered laser radiation, process emissions and vapour but primarily by the unknown emission coefficients and measuring angles between the pyrometer axis and the surface area to be probed. A novel approach for effectively measuring temperatures in the vicinity of the keyhole front wall was introduced by Pordzik and Woizeschke [18] who used frontal drillings into the weld specimen at different depths equipped with tantalum probes to form a refractory measuring channel, enabling pyrometric high-speed measurements along a path piercing through the middle of the process zone. This method is restricted by the evaporation temperature of the substrate material as the tantalum probe is required to stay intact until it is directly

exposed to laser radiation inside the keyhole so that the combination of substrate material and probe material must be chosen carefully.

In this study, the suggested method of using refractory tantalum probes to establish pyrometric measurements of the leading process zone in front of the keyhole centre has been applied to a set of process parameters resulting in different weld depths and exhibiting different process behaviours during partial-penetration welding in pure aluminium sheets (EN AW-1050A). The pyrometric measurements were accompanied by on-line measurements of the keyhole depth by means of OCT to monitor the fluctuation of the keyhole depth as a parameter for the keyhole dynamics on the one hand and on the other hand to identify certain regions of the recorded temperature profiles based on characteristic events in the keyhole depth signal beyond the accuracy of probe positioning. As the process zone moves across the tantalum probe, each region of the process zone is only captured in the measured temperature signal for a short time period, starting from the pre-running melt and ending at the moment of destruction of the probe. Therefore, as a consequence of the functioning principle of the applied method, a measurement performed on a single weld sample equipped with a tantalum probe can only yield short snapshot-like measurements of each characteristic region in the leading process zone.

2 Experimental setup and methods

2.1 Experimental setup

2.1.1 Specimen design

The weld specimens were prepared according to Pordzik and Woizeschke [18] using pure aluminium (EN AW-1050A) as substrate material in the shape of blocks with the dimensions $60 \times 40 \times 15\ mm^3$. The refractory probes consisted of high-purity tantalum Ta99.9 made from two parts, the tantalum tube acting as the refractory measuring channel and the foil acting as temperature screen. The tantalum tubes had a length of 8 mm, an outer diameter of 1.05 mm and an inner diameter of 0.6 mm. The end of the tube was covered and sealed by a tantalum foil with a thickness of 20 µm using micro deep drawing. Holes with a diameter of 1.1 mm were drilled into the frontside of the aluminium blocks at depths ranging from 2 to 5 mm in steps of 1 mm and were equipped with the tantalum probes, with the sealed side of the tube facing towards the drill hole. A schematic of the weld specimen is shown in Fig. 1b. According to [18], the tantalum foil at the end of the probe is expected to act as a direct temperature screen by projecting the temperatures on the outside of the probe onto the inner side of the foil with the advantage of emitting thermal radiation at known emission coefficients of the pure tantalum surface, thus allowing for the calculation of absolute temperatures from the recorded pyrometric voltage signal by means of a self-consistent temperature calculation. The refractory probes, after being placed in the drill holes, were centre-punched at the opening to ensure the probe's placement in the correct depth minimising possible air enclosures at the end of the drill hole and for fixation to prevent tilting during the measurements. Each specimen is only used for one weld seam as the refractory probe is destroyed during the process.

2.1.2 Experimental setup and on-line process monitoring

The weld specimens were placed in a sample holder mounted on top of a goniometer table for fine adjustments of the specimen position and tilting. For the pyrometric measurements, a narrow-band pyrometer of the type KGA 740 (Kleiber Infrared GmbH, Saalfeld, Germany) was used operating at a spectral range in the infrared spectrum between 2000 and 2200 nm recording at a sampling rate of 166 kHz. The pyrometer was calibrated for a temperature range between 350 and 3500 °C based on a black body radiation source. As the occurring emissivity values during the process are expected to be much lower than 1, corresponding to an ideal black body radiation source, the measurable temperature range is shifted towards higher temperatures according to the occurring emissivity values. The minimum size of the measuring spot was 0.4 mm at a measuring distance of 115 mm between the lens and the surface to be measured. Therefore, the pyrometer was positioned at a distance of 115 mm from the frontside of the aluminium block focusing onto the opening of the refractory probe. As pyrometers relying on a single spectral range are highly sensitive towards the measurement spot illumination, it was important to ensure exact positioning between the pyrometer and the refractory probe to obtain reliable and meaningful temperature values. The alignment between the probe and the optical axis of the pyrometer was achieved by translational shifting of the pyrometer and fine adjustment of the tilting of the weld specimen in order to accurately align the pyrometric axis with the axis of the refractory probe to ensure complete overlap between the measuring spot of the pyrometer and the tantalum foil at the end of the probe. The welding was performed using a disk laser of the type TruDisk 12,002 (Trumpf GmbH & Co. KG, Ditzingen, Germany) operating at a wavelength of 1030 nm with a minimum beam parameter product of 8 mm·mrad. The laser source was used in combination with a processing head of the type YW52 (Precitec, Gaggenau, Germany). Using a fibre core diameter of 200 µm with an aspect ratio of the processing head of 3:2, a nominal focal spot diameter of 300 µm was achieved. The Rayleigh length of the processing laser

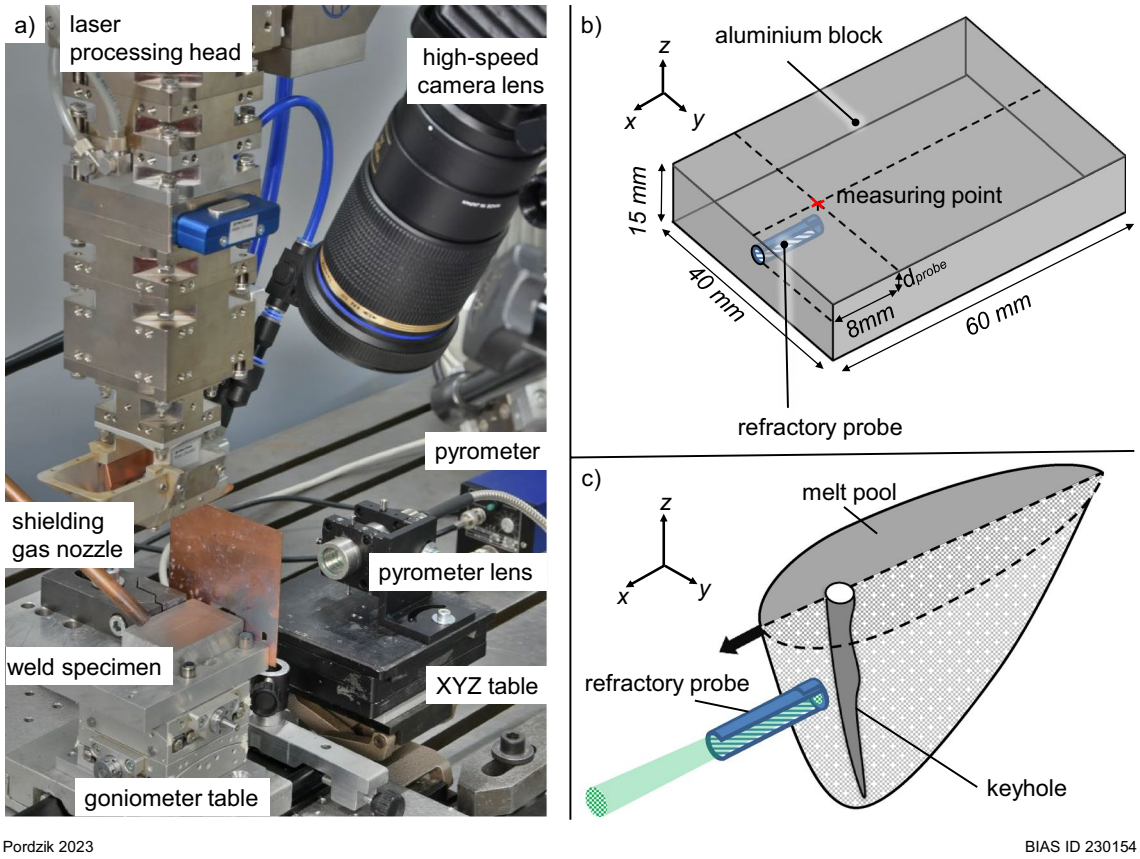

Fig. 1 Experimental setup for the conducted experiments including the processing head the weld specimen and several measuring devices (**a**). Schematic of the weld specimen consisting of an aluminium block equipped with a refractory tantalum probe (**b**). Schematic of the measuring procedure with the process zone passing over the refractory probe emitting the measured thermal radiation (**c**)

beam with a Gaussian transversal intensity profile was 2.52 mm. The angle of incidence of the processing setup was tilted by 5° to the vertical orientation against the welding direction. During the experiments, argon was used as shielding gas at a flow rate of 30.5 L/min using a nozzle diameter of 8 mm. The processing head was equipped with an OCT measuring module. The OCT probe beam was generated from a superluminescent diode (SLD) operating at a central wavelength of 1550 nm and a spectral width of 35 nm (full width at half maximum (FWHM)) with a power of 40 mW. The focal diameter of the OCT probe beam was approximately 70 µm and was directed into the keyhole coaxially to the processing laser beam. The OCT system was capable of recording at a maximum measuring frequency of 70 kHz yielding a distance value for the most pronounced scattering surface at each measurement. The signal of both measuring devices, the pyrometer and the OCT were recorded synchronously by an FPGA controller (field programmable gateway array) of the type NI cRIO-9035 (National Instruments, Austin, Texas, USA) equipped with the analogue input module NI-9222 providing a sampling rate of 500 kS/s. This way the exact temporal correlation between the pyrometric temperature signal and the depth signal from the OCT measurement was ensured. The experimental setup is shown in Fig. 1a.

The experiments were executed for different laser powers at a constant process velocity of 3000 mm/min. The laser power was chosen in such a way that deep penetration welding was achieved. Depending on the weld depth for each combination of process parameters, pyrometric measurements in depths from 2 to 5 mm were conducted in steps of 1 mm. Each experiment was repeated 5 times to account for the transient keyhole shapes that were expected to be encountered throughout the single measurements. To ensure that the obtained temperature values at a given keyhole depth are representative for the whole circumference of the keyhole, the experiments were conducted in the so-called Rosenthal regime (< 5000 m/min) as described by Fabbro, who stated a uniformly temperature distribution in the vicinity of the material evaporation temperature at this welding regime [19]. Thus, the welding experiments were conducted at a constant process velocity of 3000 mm/min. The laser power was varied between values of 4000 W and 6000 W resulting in a deep welding process. The laser focus was

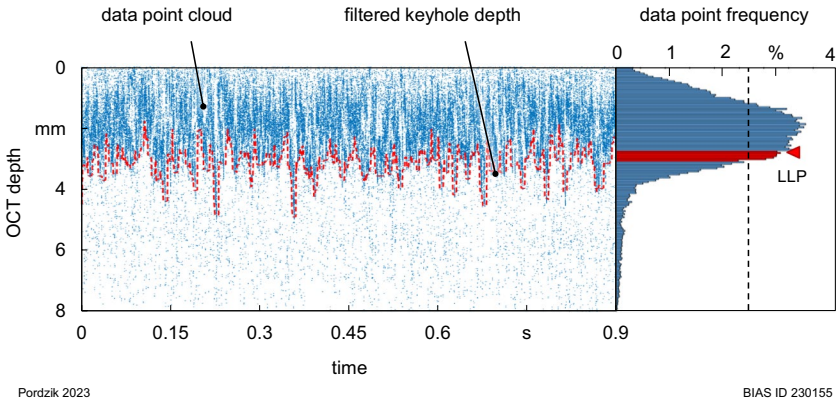

Fig. 2 OCT depth measurement signal (blue dots) of a deep welding process of pure aluminium overlaid with a time-resolved LLP depth analysis (red curve) based on the histographic analysis of the data point frequency distribution (right)

shifted from the specimen surface by a value of − 4.36 mm, therefore positioning the focal plane below the specimen surface resulting in a converging beam caustic inside the keyhole and a laser spot diameter on the specimen surface of 600 µm. Based on prior experiments, the focus shift was applied to mitigate the process dynamics for the weldment of aluminium what is considered beneficial for the applied temperature measuring technique.

2.1.3 High-speed videography of the melt pool surface

Separately for each combination of process parameters, high-speed recordings of the melt pool surface including the keyhole opening were executed using a high-speed camera of the type Photron Nova S-12 (Photron, Tokyo, Japan) in combination with the illumination laser CAVILUX HF (Cavitar Ltd, Tampere, Finland) operating at a central wavelength of 810 nm. The camera lens was equipped with a narrow bandpass filter transmitting light at a central wavelength of 810 nm with 12 nm FWHM enabling the light from the illumination laser to be recorded by the high-speed camera while protecting it from potentially harmful scattered radiation. The high-speed recordings were performed with a resolution of 600 px × 240 px at a frame rate of 100 kHz.

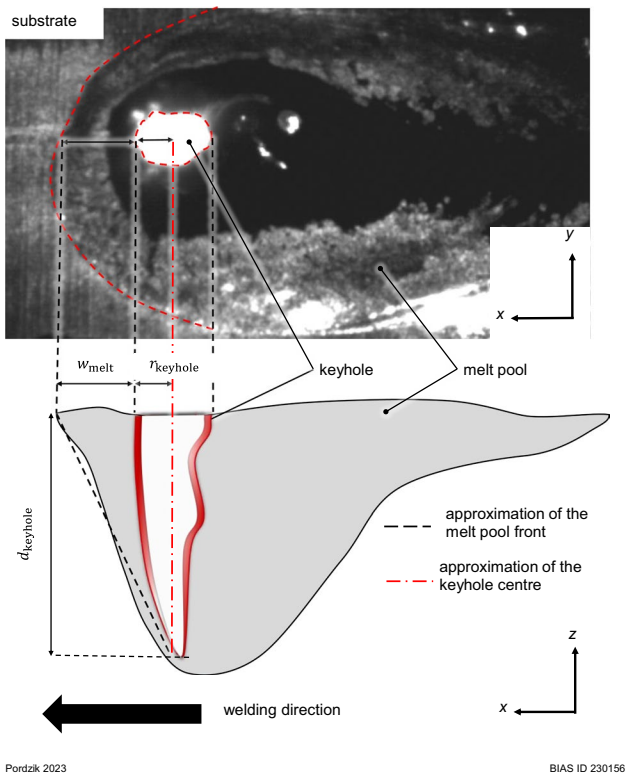

Fig. 3 Snapshot of the process zone surface supplemented with a schematic of the in-depth process zone showing the geometrical derivation of the estimated interface positions in the frontal area of the process zone

2.2 Methods

2.2.1 Analysis of the keyhole opening diameter and pre-running melt

The high-speed recordings of the process zone were analysed regarding the size of the keyhole diameter as well as the length of the pre-running melt measured between the frontal apex of the keyhole opening and the frontal apex of the melt pool front according to Fig. 3. Based on measurements in 10 different frames that exhibited sharp keyhole opening contours, the average values and the standard deviations for both quantities were calculated for each parameter set. As the employed high-speed camera uses a CMOS for sensor for light detection, distorting effects due to the overexposure like "blooming" are neglectable because these sensors are robust against overflowing charges between neighbouring pixels. The perspective distortion of the melt pool proportions caused by the inclination between the high-speed camera and the specimen surface of approximately 60° was compensated arithmetically based on images of a reference cube with known edge lengths recorded under the same conditions as the experiments.

2.2.2 OCT measurements of the keyhole depth

The OCT signal yields the most prominent depth value of each single measurement. As the OCT probe beam is directed coaxially to the processing laser beam into the keyhole, the keyhole bottom is assumed to be the strongest reflecting surface on average. Nonetheless, the pronounced process dynamics during the welding of pure aluminium disturbs the depth measurement by adding reflecting features other than the keyhole bottom to the aggregate of depth measurements yielding the demand for statistical filtering to acquire the actual keyhole depth from the recorded data point cloud. According to Mittelstädt et al. [20], the last local peak (LLP) of the histographic data point distribution is highly correlated to the metallographically obtained weld depth. Mattulat et al. implemented the histographic LLP analysis in a time-resolved manner by analysing the frequency distribution of OCT data points on a gliding window function [21]. The OCT measurements in this research were analysed applying the LLP method for extracting the keyhole depth from the OCT data point distribution as illustrated in Fig. 2. Using a window size of 2000 sampling points or 4 ms, respectively, and an overlap of 500 sampling points, a temporal resolution of the OCT keyhole depth of 1 ms was achieved. The width of the histogram bins in the LLP analysis was set to 50 µm which also constitutes the resulting depth resolution. The standard deviation of the keyhole depth is used as a measure for the keyhole depth fluctuations.

The OCT depth measurements serve two purposes. The first one is gaining information about the mean keyhole depth and the depth fluctuation at given process parameters as a measure of the process dynamics, and the second one is to detect the moment of the keyhole hitting the tantalum probe by observing a significant change in the OCT frequency distributions. Each information is used to evaluate and interpret the recorded temperature curves.

2.2.3 Temperature calculation and analysis

The raw signal of the pyrometric measurement is a voltage signal ranging from 0 to 10 V that is proportional to the detected light intensity on the photodiode of the pyrometer. Deriving a temperature curve from the raw signal requires the knowledge of the temperature- and wavelength-dependent emission coefficient of the measured surface. Additionally, as already introduced by Pordzik and Woizeschke [18], the temperature calculation becomes self-dependent as the emission coefficient itself depends on the temperature demanding for an iterative algorithm for the self-consistent temperature calculation. The self-dependent temperature calculation from the pyrometric raw signal was performed accordingly. The temperature diagrams were divided into regions before and after the estimated calculated moment of probe destruction and further divided into characteristic regions with significant resemblance between the single iterations per experiment. After the destruction of the refractory probe, the measuring conditions for the pyrometer are unknown as neither the emissivity values inside the keyhole nor the distribution of the measuring angles between the aluminium melt and the pyrometer axis is known. Furthermore, the destruction of the tantalum foil causes a shift in the focal position of the pyrometer on the newly established measuring surface at the aluminium melt front. Despite the changed measuring conditions at the moment of the destruction of the refractory probe from solid tantalum to liquid aluminium or vapour, for the whole calculation of the complete temperature curves, the emission coefficients for solid tantalum were applied. This implies that values after the moment of probe destruction only allow for qualitative analysis of the curve progression and do not yield absolute temperature values. This is indicated by the labelling of the regions before and after the estimated moment of probe destruction as valid and invalid. The calculation of the moment when the probe was expected to be destroyed by direct exposure to laser radiation was based on the high-speed imaging of the melt pool surface. According to Fig. 3, a linear approximation of the shape of the melt pool front contour (cone-like keyhole and thus the pre-running melt pool shape assumption) was assumed in order to estimate the keyhole centre in relation to the first occurrence of temperature signals in the pyrometric measurement. The first occurrence of temperature signals in the pyrometric recording channel is associated with the first contact between the tantalum probe and the pre-running melt, denoted by t_0. The depth-dependent estimation for the valid measuring time interval Δt_{meas} based on the evaluation of the high-speed recordings was then calculated according to Eq. 1. The estimated time for the keyhole centre reaching the tantalum probe t_{centre} resulting in its definitive destruction was calculated according to Eq. 2.

$$\Delta t_{\mathrm{meas}} = \frac{\overline{w}_{\mathrm{melt}} + \overline{r}_{\mathrm{keyhole}}}{\overline{d}_{\mathrm{keyhole}}} \cdot \frac{\overline{d}_{\mathrm{keyhole}} - d_{\mathrm{probe}}}{v} \tag{1}$$

$$t_{\mathrm{centre}} = t_0 + \Delta t_{\mathrm{meas}} \tag{2}$$

where $\overline{d}_{\mathrm{keyhole}}$ denotes the average keyhole depth derived from the LLP analysis of the OCT data, d_{probe} denotes the central depth position of the refractory probe below the specimen surface, $\overline{w}_{\mathrm{melt}}$ describes the average width of the area of the pre-running melt in front of the apex of the keyhole opening and $\overline{r}_{\mathrm{keyhole}}$ finally describes the average radius of the keyhole opening. The process velocity is denoted by v.

2.2.4 Spectrographic analysis of superimposed high-frequency temperature fluctuations

The temperature curves were analysed further regarding the exhibited frequencies. As shown by Pordzik and Woizeschke [18], the macroscopic features of the temperature curve progression are temporarily superimposed by fluctuations on different scales of time and magnitude. As they shift between different sections of the temperature curves, the superimposed fluctuations can be considered a characteristic feature on their own and therefore worthwhile to be analysed in detail. The fluctuations were separated from the raw signal by performing a Gaussian smoothing of the temperature curve resulting in a representation of the macroscopic curve progression. By subtracting this smoothed curve from the original temperature curve only the signal components that were erased by the Gaussian smoothing remain. The separation between the high-frequency signal fluctuation and the macroscopic curve progression is necessary to avoid frequencies resulting from the Fourier transform of macroscopic edges and steep slopes of the signal to dominate the spectrogram and thus blur the spectrographic features originating from actual signal fluctuations (Fig. 4).

For the Gaussian smoothing, a gliding window with a width of 1000 data points being equivalent to a time span of 2 ms was applied. Using a gliding Fourier transform with a window size of 2000 sampling points or 4 ms, respectively, and an overlap of 1000 sampling points between neighbouring windows for each temperature curve, spectrograms were calculated identifying the dominant frequencies in each time window. For the given time range and the temporal resolution of the FPGA controller of 2 µs, a frequency resolution of 165.3 Hz could be achieved by applying the MATLAB build-in fast Fourier transform (FFT) algorithm. For further analysis, only frequencies between 0 and 40 kHz were considered according to Nakamura and Ito; the dominant process frequencies are to be expected in the range between 1 and 4 kHz [22].

3 Results

3.1 Analysis of the keyhole depth by means of OCT

The keyhole depths at the different laser powers applied during the welding of pure aluminium at a process velocity of 3000 mm/min were evaluated according to the methodology described in Sect. 2.2.2. The results are depicted in Fig. 5. The average keyhole depth increases with increasing laser power. At a laser power of 4000 W, an average keyhole depth of 3 mm is determined while for 6000 W, the OCT signal yields an average keyhole

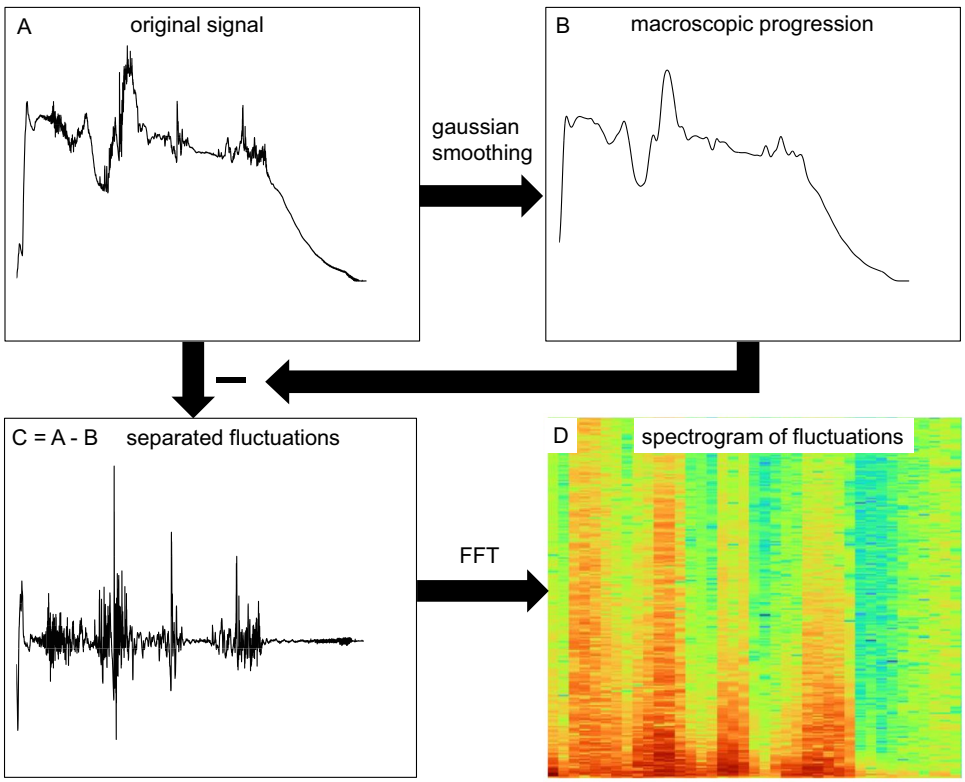

Fig. 4 Schematic of the separation of the macroscopic curve progression and the superimposed fluctuations from an original signal enabling the spectrographic analysis of the separated fluctuation pattern

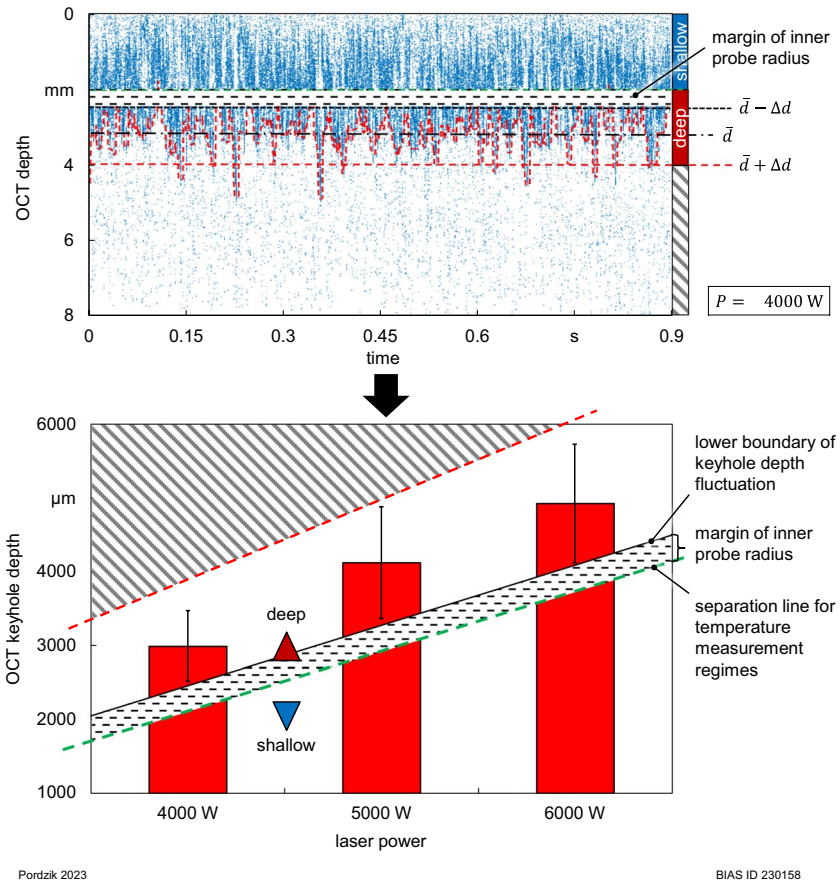

Fig. 5 Exemplary OCT signal with marked average keyhole depth and keyhole depth fluctuations based on the LLP method (top). Dependency of the average keyhole depth and the keyhole depth fluctuations on the applied laser power for welding of pure aluminium at a process velocity of 3000 mm/min including a separation between different depth regimes for the pyrometric measurements of the pre-running process zone (bottom). The area above the red dashed line indicates the depth region; the keyhole does not reach while the area below the green dashed line indicates the depth region where the keyhole is assumed to be permanently present

depth of approximately 5 mm. Furthermore, the standard deviations of the keyhole depths increase from 0.5 mm at 4000 W to 0.85 mm at 6000 W.

Regarding the pyrometric measurements of the temperatures in the leading process zone, the resulting keyhole depths from Fig. 5 are separated into three regions. The first region is the region below the lower boundary of the keyhole depth fluctuations minus the inner radius of the refractory probe indicated by the green dashed line, thus defining the region where the keyhole is expected to be permanently present at the full front of the refractory probe. In the following, this region is referred to as "shallow". The region above the upper boundary of the keyhole depth fluctuations is the region that is expected not to be reached by the keyhole and therefore would not yield any temperature measurements related to the keyhole wall. This region is marked by the shaded pattern above the red dashed line. The region in between the green and the red dashed line defines the depth range in which the keyhole fluctuations overlap the front of the refractory probe, meaning, that the keyhole front wall is not ensured to be present at the full front of the probe at any time. In the following, this depth region is referred to as "deep".

3.2 Analysis of the keyhole opening and the pre-running melt

The high-speed recordings of the melt pool including the keyhole opening were evaluated according to the description in Sect. 2.2.1. The results of the analysis are shown in Fig. 6. Both the keyhole diameter and the pre-running melt pool width increase with increasing laser power at a constant velocity of 3000 mm/min. The keyhole diameter exhibits a weak dependency on the laser power as it increases from approximately 0.8 mm at 4000 W to 0.9 mm at 6000 W with standard deviations ranging between 0.05 and 0.09 mm. The keyhole opening obtained from the high-speed recordings therefore shows diameters approximately 1.5 times as large as the diameter of the laser spot at the position of the specimen surface.

The pre-running melt at the melt pool surface shows a stronger dependency on the laser power ranging from values slightly below 0.8 mm at 4000 W to approximately 1.1 mm at 6000 W. The standard deviations for the pre-running melt of approximately 0.15 mm are significantly larger than those calculated for the keyhole diameter. Based on the approximations of the cone-like shapes of the different regions in

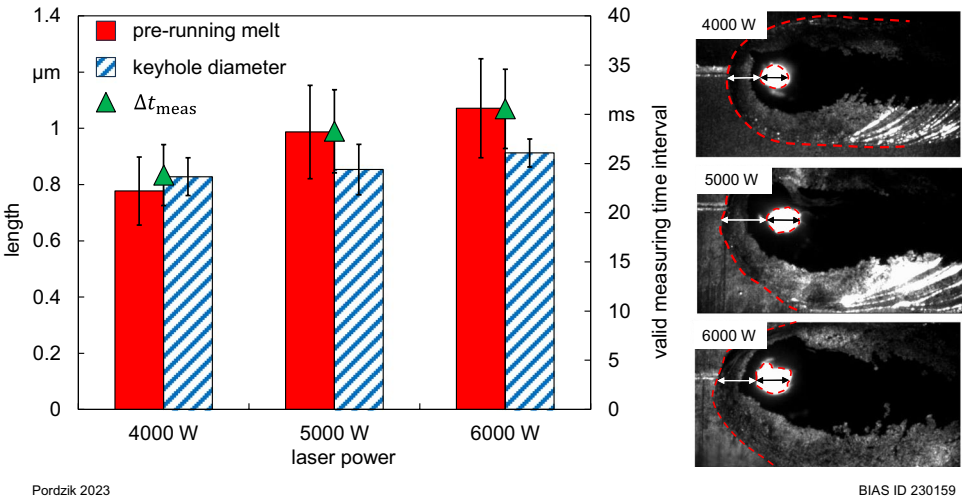

Fig. 6 Correlation between the keyhole opening diameter and the width of the pre-running melt at the melt pool surface on the laser power for welding pure aluminium at a process velocity of 3000 mm/min (left) and snapshots of the melt pool surface including the keyhole opening at different laser powers (right)

the process zone as described in Sect. 2.2.3 and shown schematically in Fig. 3, the combination of the average keyhole depth (given in Sect. 3.1), the width of the pre-running melt and the keyhole opening diameter enables the calculation of the estimated valid measuring time Δt_{meas} according to Eq. 1. This time span describes the duration from the first contact between the pre-running melt and the refractory probe at the chosen depth until the keyhole centre reaches the tip of the refractory probe, what is associated with its definite destruction. Therefore, from the observation of the first temperature measurement on, Δt_{meas} describes the time interval during which the refractory probe presumably remains intact and valid temperature measurements can take place. The values for the respective time interval depending on the process parameters are given in Fig. 6.

3.3 Pyrometric temperature measurements inside the refractory probe

From the pyrometric measurements of the tantalum foil at the end of the refractory probe, the signals are recorded and converted to absolute temperature values according to the description in Sect. 2.2.3. For the three different laser powers applied and the respective depth ranges suited for temperature measurements as described in Sect. 3.1, a different number of possible measuring depths resulted for each process parameter combination. By repeating each experiment 5 times for statistical validation of the measurement, a total number 45 measurements were recorded. At the end, 42 yielded reasonable temperature signals have been used for the analyses. Due to the large number of measurements, the qualitative progressions of the temperature signals are described exemplarily using two measurements from the two different measuring regimes. In the following, to improve clarity, the temperature measurements are centred around the estimated time of probe destruction $t_{centre} = 0$ ms; thus, the negative region on the time axis corresponds to the valid measuring interval while the positive region corresponds to the invalid one. The temperature curves are supplemented by the analysis of their superimposed high-frequency fluctuations according to the description in Sect. 2.2.4.

3.3.1 Analysis of exemplary temperature measurements obtained from "shallow" and "deep" measuring regimes

An example for a measurement carried out in the "shallow" regime is shown in Fig. 7 for a laser power of 4000 W and a process velocity of 3000 mm/min. The temperature measurement only yields values in the late state of the process when the process zone approaches the position of the tip of the refractory probe. The temperature signal exhibits an abrupt increase to values around 3000 K, already exceeding the evaporation temperature of pure aluminium. After approximately 20 ms after the occurrence of the first temperature detection, a temperature drop is observed immediately followed by the global maximum of the temperature measurement. The signal maintains temperature values above 2000 K until the final cooling down phase, where the temperature drops below the measuring range of the pyrometer. Concerning the high-frequency fluctuations of the temperature signal, alternating regions of smooth and fluctuating regions with durations between 5 and 10 ms are observed. Noticeably, the regions with pronounced high-frequency fluctuations coincide with the broad temperature peaks or spiking.

In addition to the temperature curves, the simultaneously recorded OCT signal is analysed. The data point distribution in the time interval of the temperature measurements yields significant regions. During the first milliseconds from 10 to 12 ms after the occurrence of the first temperature signal, the OCT signal is similar to the distribution during the previous

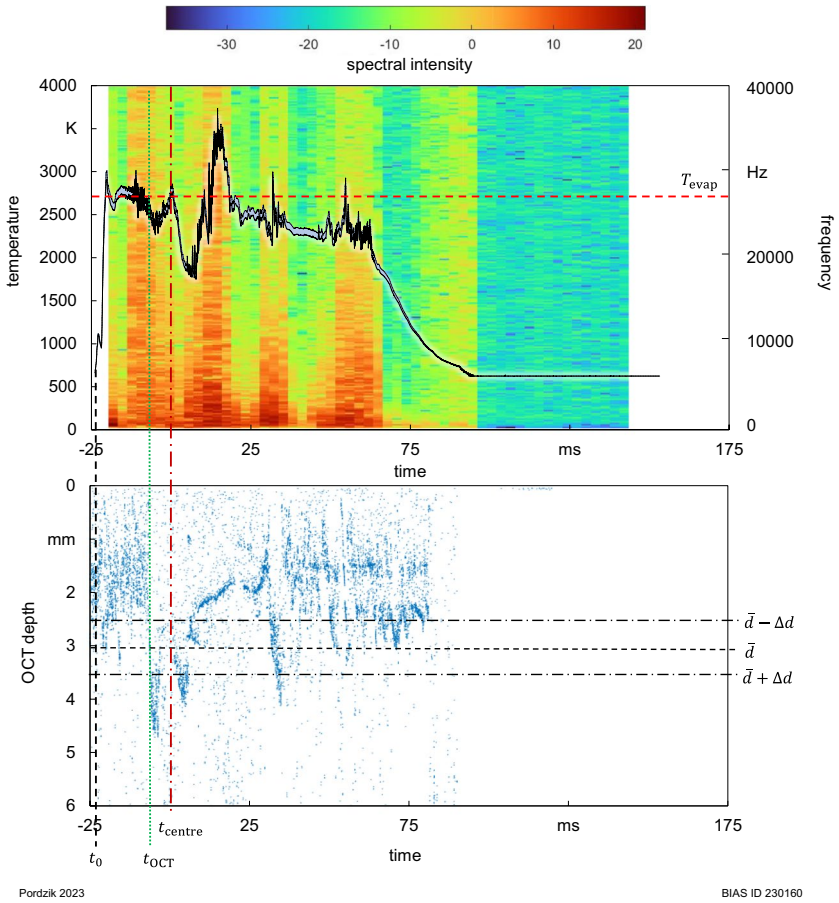

Fig. 7 Comparison between a temperature measurement from the "shallow" measuring regime including a spectrographic analysis of the signal fluctuations (top) and a synchronously recorded OCT measurement (bottom) with estimated interaction times between the refractory probe and frontal process zone interfaces and significant regions of the keyhole depth measurement

undisturbed welding process. After 12 ms, two significant spikes can be observed at a depth of approximately 4.5 mm. The data point distribution shows a high density of the accumulation indicating a strong reflecting surface in this region. The region with the two depth spikes is exactly centred around the estimated keyhole centre time. Immediately after this region, the depth value drops to 2 mm while the accumulation becomes even denser. About 30 ms after the estimated keyhole centre time, the OCT signal changes to a progression showing alternating accumulations at 1.5 mm and 2.5 mm with a broader scattering similar to the undisturbed signal, thus being centred around the central position of the refractory probe at 2 mm. The moment of change in the OCT signal between a presumably undisturbed and a disturbed region is indicated in Fig. 7 by t_{OCT}.

The different characteristic regions identified in the OCT signal were analysed histographically according to the description in Sect. 2.2.2 regarding the frequency distribution of data points, as shown in Fig. 8. The histograms yield the relative data point frequencies normalised by the overall number of OCT data points in the respective time window to improve the comparability between the different identified regions in the OCT signal. The first region (I) marks the undisturbed welding process without any interactions with the refractory probe. The histogram for the data point distribution shows a high and broad maximum, as it is usually observed for laser welding of aluminium and normal ambient pressure (see, e.g. [23]). The second region (II) denotes the rather inhomogeneous pattern after the presumably undisturbed welding process. The histogram shows three pronounced maxima at approx. 2 mm, 3 mm and 4 mm that are significantly narrower than the maximum observed in the undisturbed region, thus indicating a selective accumulation of OCT data points. The third region (III) that was identified based on the reestablished regularity of the OCT signal exhibits two sharp and pronounced maxima at depths of approximately 1.6 mm and 2.4 mm. The centre of the gap between these two peaks is at a depth of 2 mm, which is consistent with the central position of the refractory probe during this measurement.

As a second exemplary temperature curve, a measurement from the "deep" measuring regime is described. In this experiment, the welding was executed at a process velocity of 3000 mm/min with a laser power of 6000 W and a measuring depth of the refractory probe of 4 mm. At the beginning of the temperature measurement, the curve exhibits an abrupt increase up to 2200 K followed by a temperature drop to 1500 K. Both the initial increase and the first drop in

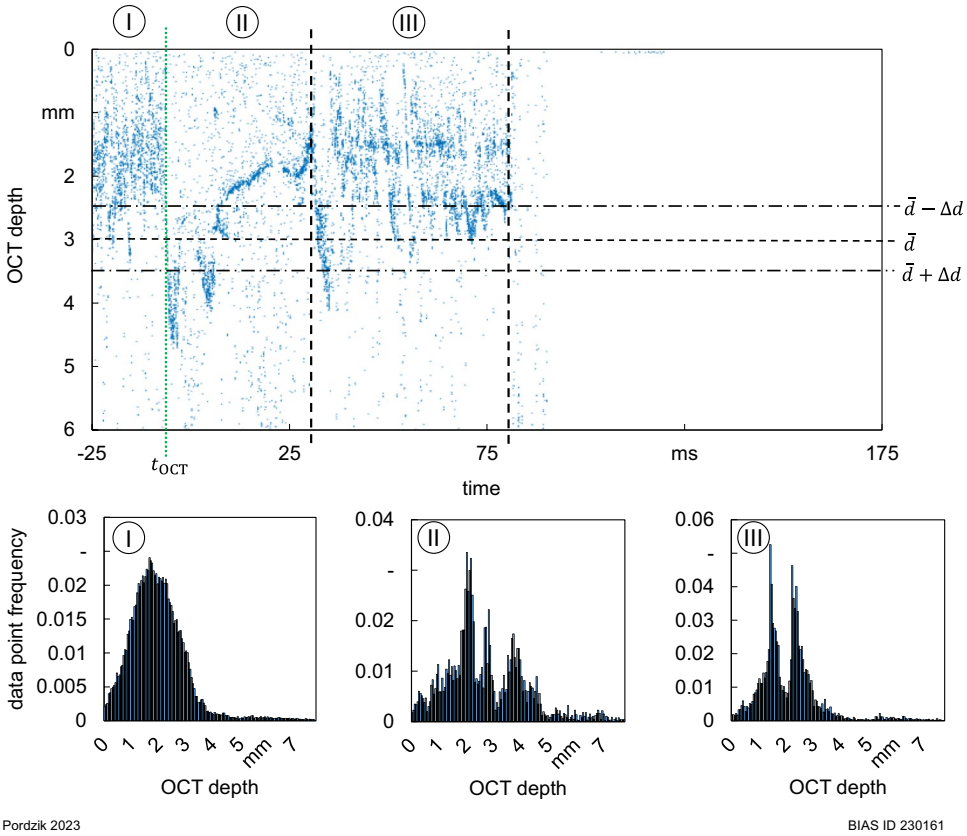

Fig. 8 Histographic analysis of different characteristic regions in the OCT signal measured synchronously to a temperature measurement at the "shallow" measuring regime

temperature have smooth progressions and no superimposed fluctuations, which is also indicated by the low-frequency excitations indicated by the spectrogram in the respective time region. The following characteristic time region ranging from − 20 to 80 ms shows a significant alternating pattern of broad temperature peaks superimposed with strong high-frequency fluctuations and followed by pronounced and smooth cooling down phases. The temperature peaks with widths between 10 and 15 ms almost always exceed the evaporation temperature of aluminium. From 80 ms to the end of the measurement, the final cooling down phase is observed while only the high-temperature region of the cooling down is smooth. Afterwards, macroscopic artefacts are observed in the low-temperature region (Fig. 9).

The corresponding OCT signal shows characteristics being very similar to the previously described "shallow" measurement. The disruption of the OCT signal is observed at − 10 ms and followed by a significant depth peak. The moment of the disruption of the OCT signal t_{OCT} coincides with the rising edge of the first broad temperature peak exceeding the evaporation temperature of aluminium. After the depth peak, lasting for approximately 10 to 12 ms, strong accumulations are observed in depths between 4.5 and 5.5 mm. After 40 ms, an alternating pattern of data point accumulations is observed with gravitational centres of the accumulations between 3.5 and 4.5 mm centred around 4 mm, which corresponds to the centre position of the refractory probe. During the cooling down phase, the OCT signal drops to 0 mm, which indicates the shut-off time of the processing laser resulting in a final collapse of the keyhole.

The OCT signal obtained from the "deep" measurement region exhibits similar characteristics as the one obtained from the "shallow" region (Fig. 10). Therefore, the signal can be segmented accordingly. The first region (I), representing a signal portion of the undisturbed weld process, shows a bulky data point distribution with low pronounced local maxima superimposed on the bulk. The highest maximum is located at 3.5 mm whereas further lower maxima are encountered at approximately 4.5 mm and 5.5 mm. The second region (II) that is defined analogously to the "shallow" measurement shows two extremely sharp and pronounced maxima at 4.5 mm and 4.8 mm with a comparably homogeneous distribution for all other depths. The third region (III) shows two broad data point accumulations. The first ranges from 2 to 3.5 mm and the second from 4.5 to approximately 6.5 mm, respectively. The first accumulation exhibits an extremely high and narrow peak at the end at 3.5 mm, while the second accumulation starts with a similarly pronounced peak at 4.5 mm. The significant gap in between these regions is located at approximately 4 mm, thus coinciding with the central position of the refractory probe.

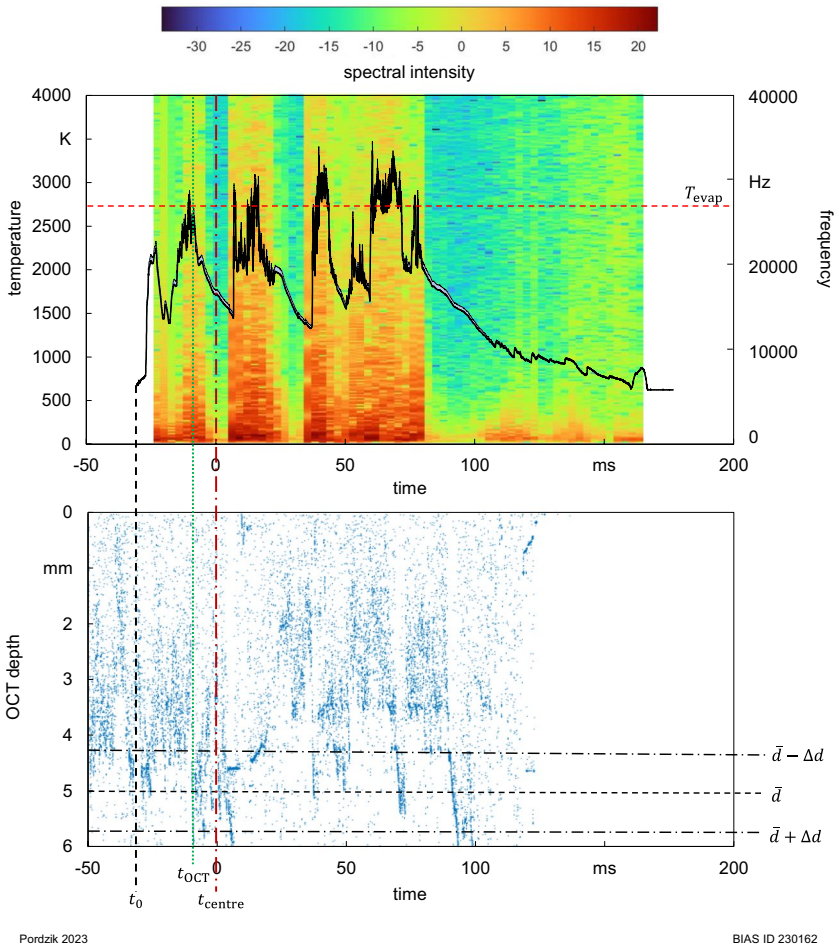

Fig. 9 Comparison between a temperature measurement from the "deep" measuring regime including a spectrographic analysis of the signal fluctuations (top) and a synchronously recorded OCT measurement (bottom) with estimated interaction times between the refractory probe and frontal process zone interfaces and significant regions of the keyhole depth measurement

Noticeably, for the regions I and III from the frequency analyses of the OCT data point distributions, the "shallow" and "deep" measurements exhibit remarkable similarities in their qualitative shapes showing a single bulky and broad accumulation for the region I and two pronounced and sharply defined peaks for the region III with a gap of approximately 1 mm in between. The region II is very different for both measuring regimes and, thus, does not exhibit any noticeable similarities except for differing widely from the regions I and III regarding the qualitative shapes.

3.3.2 Valid temperature curve sections obtained at the "shallow" measuring regime

To further elucidate and analyse the signal characteristics resulting from the applied temperature measuring method, it is necessary to apply some of the assumptions, introduced in Sect. 2.2, in order to restrict the analysis of the extensive temperature measurements to potentially meaningful time intervals. Therefore, an overview over the temperature progressions of measurements obtained from the measuring depths defined as "shallow" is given in Fig. 11. The range of the time intervals for the depicted measurements is limited to the time span from t_0 to t_{centre}, in which the refractory probe is expected to remain intact and yield meaningful temperature values according to the measuring principle. The small Roman letters in Fig. 11 indicate the repetition number for an experiment, while the Arabic numbers indicate the different process and measuring parameters that are listed in Table 1. Additionally, the time of the disruption of the OCT signal t_{OCT} is shown for each measurement, where such a disruption could be observed, and the evaporation temperature of pure aluminium T_{evap} is marked in the graphs.

From the compilation of valid temperature regions shown in Fig. 11, it can be seen that in the beginning of every temperature measurement except for the measurement 4-(ii), the curves exhibit a smooth progression with no or at most small fluctuations on short time scales. During these initial phases, the temperatures do not exceed the evaporation temperature of aluminium. The smooth region is most often followed by a region of high temperatures superimposed with strong signal fluctuations. The distinction between a smooth and a fluctuating curve progression is made according to Fig. 4, where the time scale of the fluctuations is defined by the specified window size of the Gaussian smoothing. Thus, the curves depicted in Fig. 11 can be segmented into regions

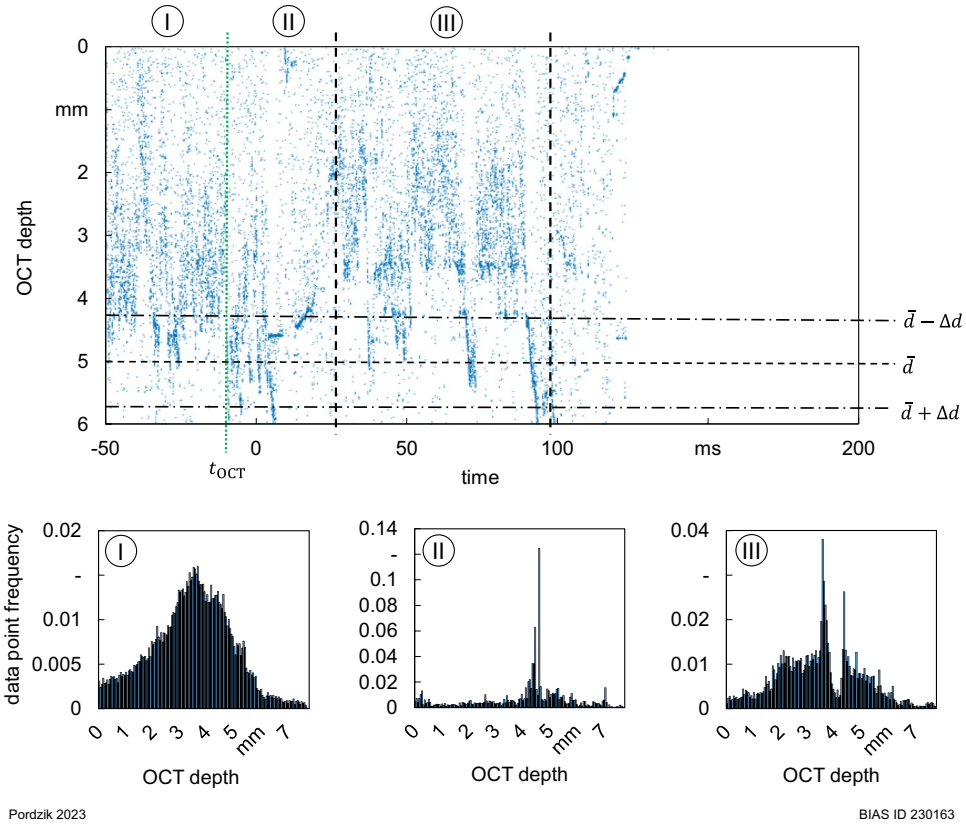

Fig. 10 Histographic analysis of different characteristic regions in the OCT signal measured synchronously to a temperature measurement at the "deep" measuring regime

with and without fluctuations on short time scales. For the sake of clarity, the spectrograms of the fluctuations have been excluded from the graphs in Fig. 11. Noticeably, the regions exceeding the evaporation temperature of aluminium are always accompanied by strong fluctuations of the signal. Furthermore, for the given time interval of the temperature curves, once high-frequency fluctuations occur in the signal, they remain until the estimated keyhole centre time t_{centre}. Most of the displayed temperature curves exceed the evaporation temperature of aluminium, sometimes even by more than 500 K. Some of the curves, e.g. 2-(i) and 2-(ii), show significant temperature spikes on top of the fluctuating high-temperature plateaus with spike heights between 400 and 800 K lasting for 1 to 2 ms. According to the analysis of the OCT signal from Sect. 3.3.1, the OCT disruption time t_{OCT} was determined and marked in the respective plots in Fig. 11 by the vertical green dashed line for each measurement. Noticeably, any disruption time that could be identified in the OCT signals is located inside the time interval Δt_{meas}. For most of the diagrams, the OCT disruption time lies either at the beginning of the high-temperature regions with strong signal fluctuations or in the centre of those regions. In the measurement 1-(iii), the OCT disruption coincides with a smooth and pronounced cooling down phase of the temperature curve making it very different from all other observations. The measurements 2-(iii) and 3-(iii) are exceptions where the OCT disruption time is located right before a pronounced smooth temperature maximum that does not exceed the evaporation temperature. For all measurements, the temperature values exceed 2000 K for most of the time and maximum temperatures of above 2500 K are observed for all measurements at least for a short period.

3.3.3 Valid temperature curve sections obtained at the "deep" measuring regime

The valid measurement region for temperature curves obtained from the depth region characterised as "deep" shows much more heterogeneous progressions and exhibits less similarities. For the sake of clarity, only the diagrams for a single experiment carried out at a process velocity of 3000 mm/min and a power of 5000 W are analysed. An overview over the parameter combinations and measuring depths is given in Table 2. The temperature curves are shown in Fig. 12. All temperature curves start with an abrupt temperature increase to temperatures above 2500 K. In most of the measurements, the initial temperature even reaches or exceeds the evaporation temperature of aluminium. Contrary to the "shallow" measurements, the curves initially already exhibit strong high-frequency fluctuations. The initial high-temperature plateaus are followed by long and smooth cooling down phases, where the temperatures drop

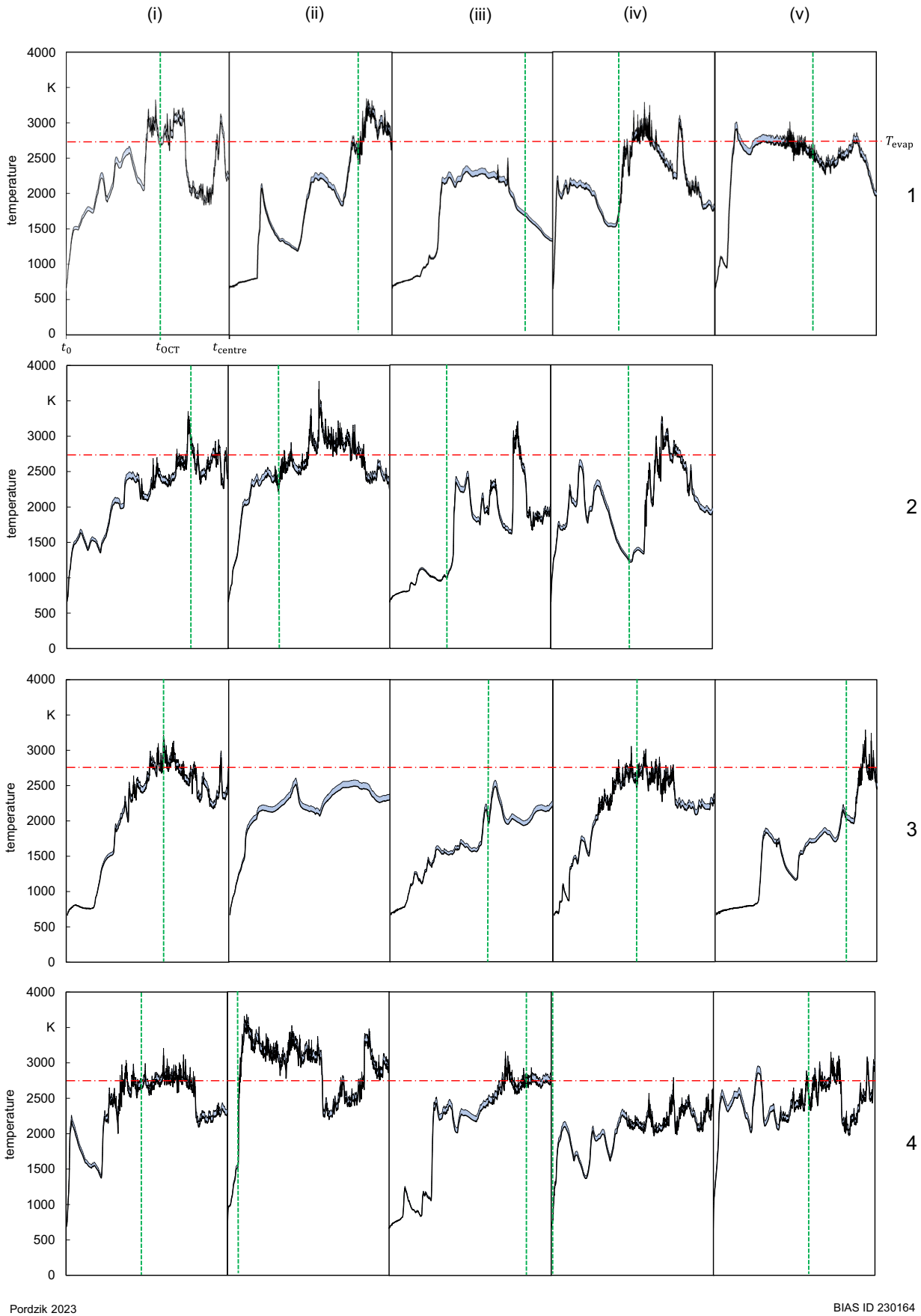
(i)
(ii)
(iii)
(iv)
(v)
temperature
4000
K
3000
2500
2000
1500
1000
500
0
T_{evap}
t_0
t_{OCT}
t_{centre}
1
2
3
4
Pordzik 2023
BIAS ID 230164

◂**Fig. 11** Compilation of valid temperature measuring intervals obtained at the "shallow" depth regime

to values below 1500 K or even below 1000 K in some cases. In some measurements, the cooling down phase lasts until the end of the valid measurement region, while in all other measurements, abrupt temperature increases reoccur that are again superimposed by strong high-frequency fluctuations and most often exceed the evaporation temperature of aluminium. The OCT disruption time obtained from the simultaneously recorded OCT signal is way more ambiguous than for the "shallow" measurements. In three cases, the position of t_{OCT} is similar to the "shallow" measurements, where the disruption time is located inside the first high-temperature plateau. Nonetheless, the correlation between the OCT disruption time and characteristics of the temperature curves is too weak to allow for generalisation.

4 Discussion

4.1 Discussion of the geometric approximations of the process zone

The high-speed recordings of the melt pool surface give access to important quantities such as the width of the pre-running melt and the keyhole opening radius. For the determination of the keyhole melt, an intensity threshold was applied, separating the bright region of the keyhole opening from the dark melt pool that surrounds it. Due to the overexposure in the region of the keyhole opening, an uncertainty about the actual keyhole opening diameter remains as overexposure might also result from back-reflections of the illumination laser from undesirable reflection angles at the curved keyhole edge or swellings in the immediate vicinity. Therefore, the obtained values for the keyhole opening diameter represent an upper boundary for the actual value. The width of the pre-running melt is affected implicitly by the uncertainty of the keyhole diameter as the width is measured from the melt pool border to the frontal apex of the keyhole opening. Nonetheless, a keyhole diameter of approximately 1.5 times the size of the laser spot diameter at the specimen surface seems plausible. The simplifications for the assumed cone-like shape of the melt pool front inside the process zone were made to give an initial orientation for distinguishing between the valid and the invalid temperature measuring regions. It is not clear whether these approximations are in good agreement with the real melt pool front contour or if the deviations are significantly large. From a physical evaluation, it seems plausible that the width of the pre-running melt is largest at the melt pool surface as the surface represents an isolating thermal boundary condition with respect to heat conduction; thus, the volume for the pre-running heat to dissipate into is smallest at the melt pool surface and increases with increasing depth in the bulky specimen. Following this argumentation, it is plausible that at high depths, the pre-running melt is thinner than the approximation would suggest. Nonetheless, such an error would not be critical for the specification of the valid measuring region as any deviation would result in an overestimation of the valid measuring interval Δt_{meas}, thus conserving all relevant regions from the temperature signal. Further experimental evaluation of the pre-running melt pool contour would allow for a more detailed and accurate specification of the valid measuring region. Furthermore, the stability of the melt pool contour in terms of temporal fluctuations is another aspect that could blur the estimated characteristic measurement time t_{centre}.

4.2 Interpretation of the OCT signals

As emphasised in Figs. 8 and 10, the keyhole depth measurement carried out during each experiment can be segmented into different characteristic regions depending on the accumulation and distribution of OCT data points. In the first region of the temperature measurement, the OCT signals seem to be undisturbed by the presence of the refractory probe. As the OCT probe beam probes the inside of the keyhole, this means that at this moment in time the refractory probe has not entered the keyhole yet, leading to the conclusion that this part of the temperature curve must originate from the contact between the probe and the pre-running melt. The interruption of the undisturbed process region indicates the interaction between the refractory probe and the keyhole or at least a disturbance of the keyhole shape caused by the presence of the refractory probe in the process zone. At this moment or at least in its immediate vicinity, the tantalum foil is expected to interact directly with the evaporation layer at the keyhole front wall. The temperature measurements of the keyhole wall and the Knudsen layer, respectively, therefore would be located in the transition area between the two OCT depth regions II and III as introduced in Sect. 3.3.1. In the following region after the assumed interaction zone between the keyhole and the refractory probe, the strong horizontal data point accumulations described in Sect. 3.3.1 occur. Noticeably, these accumulations, while being regularly interrupted by depth spikes and noisy patterns, are located at the positions of the probe walls centred around the measuring depth with an offset of half the diameter of the refractory probe in each direction. In this last region, these patterns last until the end of the welding process suggesting that the welding through the destroyed refractory probe is observed. This assumption is strongly supported by the histographic analyses shown in Figs. 8 and 10. The frequency distributions from region III show

Table 1 Process and measuring parameters for the temperature measurement compilation from the "shallow" depth regime

Row number in Fig. 11	1	2	3	4
Laser power in W	4000	5000	6000	6000
Process velocity in mm/min	3000	3000	3000	3000
Keyhole depth in mm	3 ± 0.6	4 ± 0.7	5 ± 0.8	5 ± 0.9
Measuring depth in mm	2	2	2	3

Table 2 Process and measuring parameters for the temperature measurement compilation from the "deep" measuring regime

Row number in Fig. 12	1	2
Laser power in W	5000	5000
Process velocity in mm/min	3000	3000
Keyhole depth in mm	4 ± 0.7	4 ± 0.8
Measuring depth in mm	3	4

strong accumulations at the positions of the upper and lower wall of the refractory probe with a pronounced gap in between. The identification of region III is important as it defines the post-measurement region and allows for better estimation of the interaction phase (II). It furthermore yields evidence that the OCT measurement is indeed capable of measuring specific recognisable geometric features of the tantalum probe. This supports the assumption that valid information about the presence of the probe tip inside the keyhole can be directly obtained from the OCT measurement although those signals do not yield recognisable features from the probe design. The interpretation of the OCT signals gives a useful framework for further interpretation of the temperature curves as they yield plausible estimations for the moments of the beginning and the end of the interaction between the keyhole and the tip of the refractory probe. The time of the disturbance of the OCT signal inside of the previously identified valid

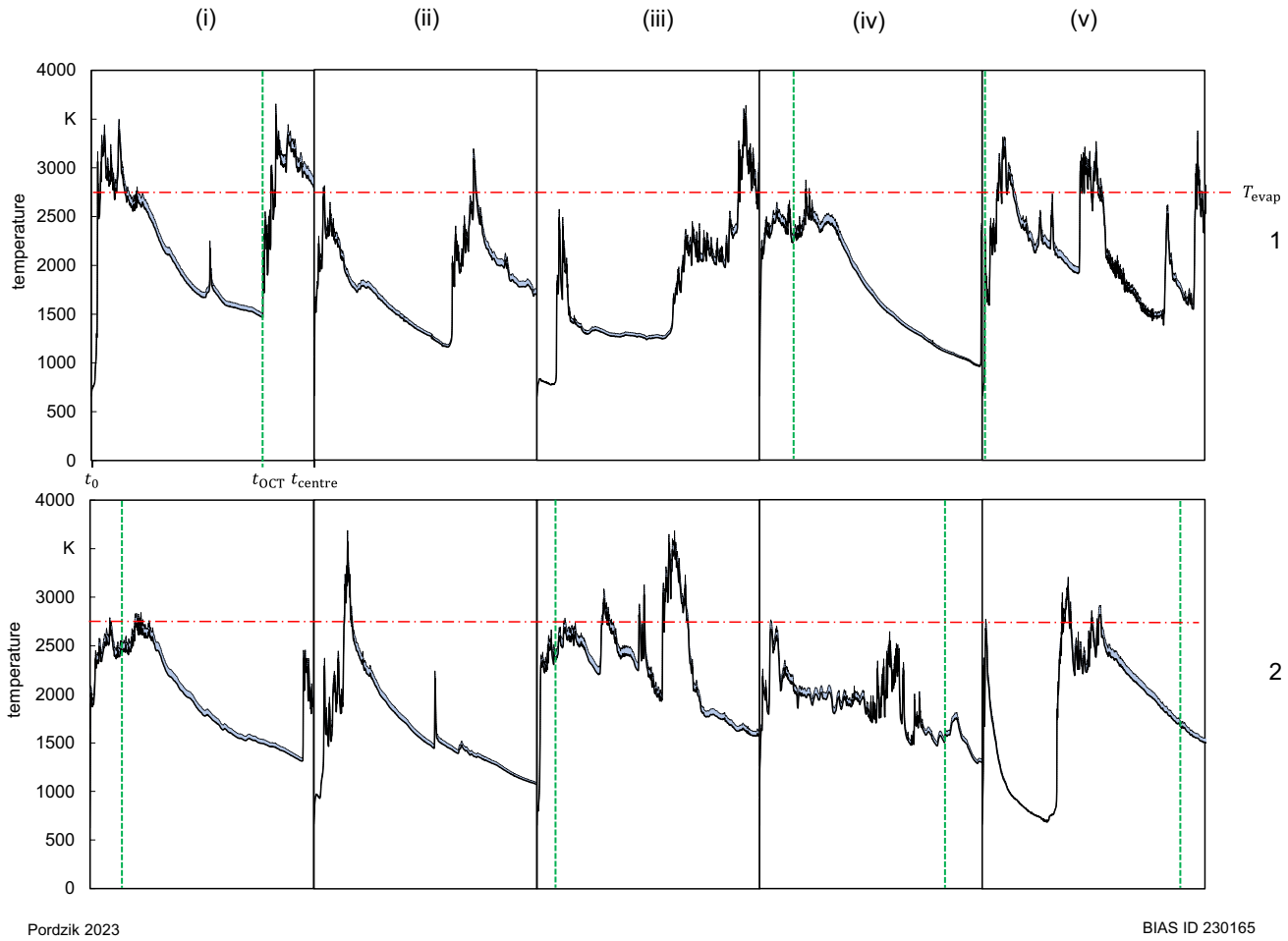

Fig. 12 Compilation of valid temperature measuring intervals obtained at the "deep" measuring regime at a process velocity of 3000 mm/min and a laser power of 5000 W

measuring region is therefore a valuable orientation mark for identifying the key wall temperatures in the pyrometric temperature signal.

4.3 Interpretation of the temperature signals

Considering the previous findings, the interpretation of the temperature curves is based on three different insights on the measuring conditions inside the process zone:

1. The OCT depth analysis in combination with the positions of the refractory probes and the measuring depth, respectively, allow for a distinction between measuring regimes that are classified as "shallow" and "deep" according to the results presented in Sect. 3.1. The "shallow" regime is expected to yield more reliable temperature values for the keyhole front wall as full contact between the keyhole wall and the front of the refractory probe is ensured at any given time relying on the keyhole depth fluctuations derived from the LLP method (Sect. 2.2.2).
2. The analysis of the high-speed recordings of the process zone surface allows estimations of the duration of the valid measuring interval Δt_{meas} using geometric simplifications of the process zone and assuming an almost straight keyhole axis due to slow process velocities and the applied beam inclination. The results described in Sect. 3.2 therefore enable the identification of a presumably valid temperature measuring interval, in which the refractory probe should remain intact leading to a drastically reduced temperature curve section left for interpretation.
3. The detailed analysis of the OCT signal recorded synchronously during the temperature measurements, as described in Sect. 3.3.1, yields a plausible time value for direct interaction between the keyhole and the refractory probe based on a significant disturbance in the OCT data point distribution. The time t_{OCT} gives a valuable hint on the actual position of the keyhole front wall.

Based on these guidelines, especially the temperature measurements obtained from the "shallow" measuring regime seem promising to yield reliable results about the temperatures inside the leading process zone. The results of the "shallow" temperature measurements, as presented in Sect. 3.3.2, are especially significant in terms of the correlation between fluctuations of the temperature curves and the temperature values themselves. Starting with smooth progressions in the first part of the valid measuring intervals well below the evaporation temperature of the specimen material, the temperature reaches and exceeds the evaporation temperature of aluminium and exhibits strong high-frequency fluctuations that last until the estimated keyhole centre time t_{centre}. Furthermore, the OCT disruption time t_{OCT} associated with the direct keyhole probe interaction coincides well with the beginning or the middle of the fluctuating high-temperature plateaus. These observations imply that the smooth curve sections before the OCT signal disruption originate from the pre-running melt while the start of the signal fluctuations in the vicinity of the OCT disruption time indicates the contact with the keyhole itself. It can be theorised that the high-frequency fluctuations of the temperature signal originate from the keyhole oscillations being transferred to the tantalum foil of the refractory probe as already implied by Pordzik and Woizeschke [18]. However, the oscillations of the probe or the tantalum foil could not be determined experimentally. It remains arguable whether the temperature maxima in these regions originate from the keyhole wall or from the direct irradiation of the tantalum foil at the tip of the refractory probe already. As the tantalum foil has a thickness of only 20 µm, the direct interaction with the laser beam would only be detectable during a very short time period resulting in a discontinuity of the temperature signal as, for example, a spike. The pronounced high-temperature plateaus on the other hand last for more than 5 ms being equivalent to a distance of 250 µm when welding at a velocity of 3000 mm/min. As this signal duration covers a region much wider than the thickness of the tantalum foil, it can be argued that the temperature values obtained from these sections indeed correspond to physical quantities in the immediate vicinity of the keyhole front wall. The assumed correlation between the temperature signal and the relative position between the probe and the process zone is shown in Fig. 13.

The temperature measurements obtained from the "deep" measuring regime are difficult to be interpreted as they do not exhibit characteristic similarities and show very different curve progressions (Sect. 3.3.3). Nonetheless, a few aspects should be discussed. First of all, no smooth temperature regions are observed at the beginning of the measurement indicating very little or no temperature measurement taking place in the pre-running melt, rather two different progressions can be distinguished. The first one starts with a broad fluctuating high-temperature plateau yielding temperatures from slightly below the evaporation temperature of aluminium up to values exceeding the evaporation temperature by up to 800 K. The second progression shows very narrow and abrupt temperature spikes followed by long cooling down phases. Noteworthy is the absence of smooth temperature regions below the evaporation temperature of aluminium indicating that, based on the interpretations of the "shallow" measurements, the refractory probe does not establish frontal contact with the pre-running melt. For this observation, two explanations seem plausible. The first explanation is a drastic overestimation of the pre-running melt at higher depths in the process zone by the geometric simplification as

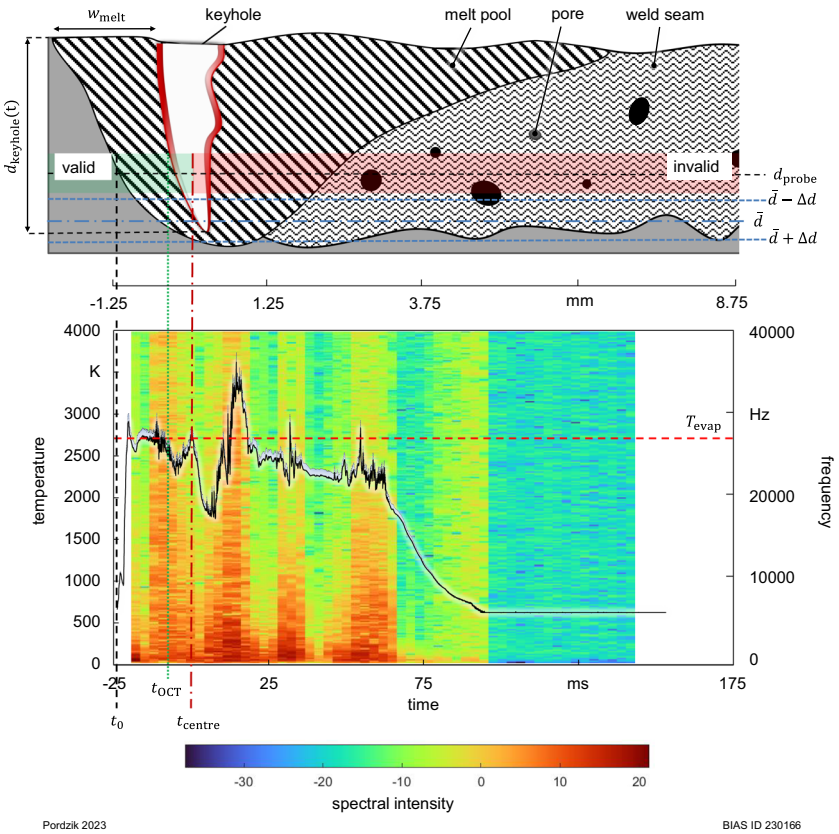

Fig. 13 Assumed spatial and temporal correlation between the temperature measurement in the leading process zone and the respective region inside the process zone illustrated by a schematic of a longitudinal cross-section through the process zone (top) and the aligned temperature measurement obtained with a refractory probe including a spectrographic analysis of the superimposed signal high-frequency fluctuations (bottom)

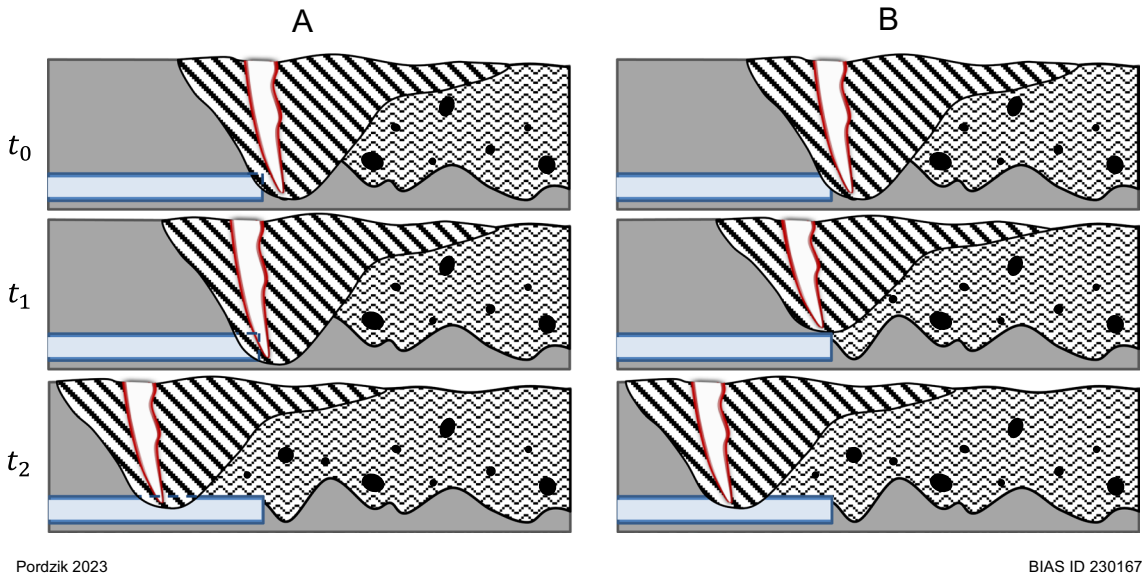

Fig. 14 Schematic progression of the measuring process in the "deep" measuring regime showing a successful progression with the keyhole front wall establishing direct contact with the refractory probe at t_1 (**A**) and an unsuccessful progression where the keyhole front misses the probe at t_1 due to its fluctuation (**B**) with both progressions indicating the possibility of the occurrence of new temperature maxima due to piercing of the refractory probe by the keyhole tip from above at t_2

shown in Fig. 3. The second explanation is a scenario, where the keyhole and the whole process zone miss the tip of the refractory probe, as shown schematically in Fig. 14. Here, the progression denoted by the letter A shows a successful measuring scenario at "deep" measuring regimes, whereas the progression denoted by the letter B shows the previously described scenario of missing the refractory probe due to keyhole depth fluctuations. The deeper the refractory probe is positioned inside the weld specimen, the more likely the scenario B would occur.

If the probe front is missed by the keyhole, temperature curves could still be recorded caused by piercing of the tantalum tube by the keyhole tip, allowing melt and molten tantalum to enter the measuring channel and electromagnetic process emissions to be measured. The two measurement series described in Sect. 3.3.3 are recorded from weld experiments using the same process parameters, therefore only differing in their respective measuring depths. Following the argumentation above, the deeper measurements would be more likely to yield temperature signals resulting from probe piercing than from frontal probe contact with the keyhole wall. For the deeper measuring region, two measurements can be identified with very narrow and high peaks immediately followed by a long and pronounced temperature drop. An explanation for this observation would be melt entering the measuring channel, pre-running inside the measuring channel and cooling down. After a while, the process zone catches up with the melt inside the channel and remelts the region, thus resulting in a periodically reoccurring alternation between abrupt temperature increase and pronounced cooling down phases as observed in Fig. 7 inside the invalid measuring region. Nonetheless, the cooling down phases are also observed after the high-temperature plateaus; thus, the exact processes resulting in the analysed temperature curves at the "deep" measuring regime until now remain speculative. In most of the experiments, temperatures exceeding the evaporation temperature of the substrate materials are measured during the valid measurement intervals. These temperatures can possibly arise due to an overheating of the melt as predicted by Ki et al. [14]. The evaporation pressure acting onto the keyhole walls leads to an increase in evaporation temperature compared to atmospheric pressure resulting in an overheating of the melt in the vicinity of the keyhole walls.

5 Conclusions

In this study, a method for measuring temperatures in the frontal process zone during laser deep penetration welding of pure aluminium was evaluated using a set of different laser powers for welding in the Rosenthal regime at a process velocity of 3000 mm/min. This method especially aims at gaining access to temperatures in the vicinity of the keyhole front wall. The measurements were performed at different depths for each combination of process parameters to record an axially resolved temperature profile. Supplementing the temperature measurements with OCT-based keyhole depth measurements and high-speed recordings of the process zone surface allowed an approximation of the time, when the refractory probe was destroyed, identifying the valid regions of measurements. From the analyses and interpretations of the obtained temperature curves, the following conclusions could be drawn:

- The analysis of the keyhole depth and its fluctuations by means of OCT allow the distinction between two depth regimes for temperature measurements, where the "shallow" region above the keyhole fluctuation range exhibits characteristic similarities between individual measurements.
- From the simultaneously recorded OCT signals in the regions of the temperature measurements, a clear interaction between the keyhole and the refractory probe can be observed allowing for interpretations of the measuring signals. The smooth temperature regions that are accompanied by undisturbed OCT measurements can be attributed to temperatures originating from the pre-running melt while the measurements taken from the disturbed region must be correlated to the immediate vicinity of the keyhole.
- Before the definitive destruction of the refractory probe, temperatures above 3000 K, therefore exceeding the evaporation temperature of the specimen material, were observed for measurements in the "shallow" regime for each combination of process parameters.
- Temperature measurements obtained from the "deep" measuring regime show no significant similarities and are not suitable to attribute specific temperatures to certain regions or phenomena in the process zone.
- In order to establish a reliable temperature measurement, the probing depth must be smaller than the lower boundary of the keyhole depth fluctuation to make sure that the tantalum foil at the probe front is covered completely by the keyhole wall rather than being pierced by the keyhole tip.
- When welding in the Rosenthal regime, the turbulent nature of the process dynamics is a challenging factor and currently limits the capabilities of measuring the keyhole front wall. Thus, it is arguable whether snapshot measurements of the keyhole front wall temperature yield the potential of providing statistically significant values for the temperature distribution at the keyhole wall.

Funding Open Access funding enabled and organized by Projekt DEAL. This research was funded by the German Research Foundation under the project number 331150978.

Declarations

Conflict of interest The authors declare no competing interests.

Disclaimer The responsibility for the content of this publication lies with the authors.

References

1. Svenungsson J, Choquet I, Kaplan A (2015) Laser welding process - a review of keyhole welding modelling. Phys Procedia 78:182–191
2. Hügel H, Graf T (2009) Laser in der Fertigung: Strahlquellen, Systeme, Fertigungsverfahren, 2nd edn. Vieweg + Teubner, Wiesbaden
3. Kawahito Y, Matsumoto N, Abe Y, Katayama S (2011) Relationship of laser absorption to keyhole behavior in high power fiber laser welding of stainless steel and aluminum alloy. J Mater Process Technol 211:1563–1568
4. Klein T, Vicanek M, Simon G (1996) Forced oscillations of the keyhole in penetration laser beam welding. J Phys D: Appl Phys 29:322–332
5. Berger P, Hügel H, Graf T (2011) Understanding pore formation in laser beam welding. Phys Procedia 12:241–247
6. Matsunawa A, Seto N, Mizutani M, Katayama S (1998) Liquid motion in keyhole laser welding, in: E. Beyer (Ed.). Proceedings of the Laser Materials Processing Conference: November 16 - 19, 1998, Sheraton World Resort Hotel, Orlando, FL, USA], [presented at] ICALEO '98, LIA Laser Institute of America, Orlando, Fla., G151-G160
7. Otto A, Koch H, Leitz K-H, Schmidt M (2011) Numerical simulations - a versatile approach for better understanding dynamics in laser material processing. Phys Procedia 12:11–20
8. Semak V, Matsunawa A (1997) The role of recoil pressure in energy balance during laser materials processing. J Phys D: Appl Phys 30:2541–2552
9. Fetzer F, Hagenlocher C, Weber R, Graf T (2021) Geometry and stability of the capillary during deep-penetration laser welding of AlMgSi at high feed rates. Opt Laser Technol 133:106562
10. Matsunawa A, Kim J-D, Seto N, Mizutani M, Katayama S (1998) Dynamics of keyhole and molten pool in laser welding. J Laser Appl 10:247–254
11. Jin X, Berger P, Graf T (2006) Multiple reflections and Fresnel absorption in an actual 3D keyhole during deep penetration laser welding. J Phys D: Appl Phys 39:4703–4712
12 Volpp J (2012) Investigation on the influence of different laser beam intensity distributions on keyhole geometry during laser welding. Phys Proc 39:17–26
13. Finke BR, Simon G (1990) On the gas kinetics of laser-induced evaporation of metals. J Phys D: Appl Phys 23:67–74
14. Ki H, Mazumder J, Mohanty PS (2002) Modeling of laser keyhole welding: part II. simulation of keyhole evolution, velocity, temperature profile, and experimental verification. Metall Mat Trans A 33:1831–1842
15. Bautze T, Kogel-Hollacher M (2014) Keyhole depth is just a distance. LTJ 11:39–43
16. Boley A, Weber G (2013) X-Ray and optical videography for 3D measurement of capillary and melt pool geometry in laser welding. Phys Procedia 41:488–495
17. Kaplan AFH, Matti RS (2015) Absorption peaks depending on topology of the keyhole front and wavelength. J Laser Appl 27:S29012
18. Pordzik R, Woizeschke P (2020) An experimental approach for the direct measurement of temperatures in the vicinity of the keyhole front wall during deep-penetration laser welding. Appl Sci 10:3951
19. Fabbro R (2010) Melt pool and keyhole behaviour analysis for deep penetration laser welding. J Phys D: Appl Phys 43:445501
20. Mittelstädt C, Mattulat T, Seefeld T, Kogel-Hollacher M (2019) Novel approach for weld depth determination using optical coherence tomography measurement in laser deep penetration welding of aluminum and steel. J Laser Appl 31:22007
21. Mattulat T, Pordzik R, Woizeschke P (2021) OCT-Einschweißtiefenüberwachung bei Unterdruck/OCT-based weld penetration monitoring at reduced ambient pressure – influence of reduced ambient pressure on the OCT signal quality in laser deep penetration welding, wt Werkstattstechnik online 111:863–868
22. Nakamura S, Ito Y (2003) Frequency analysis of optical and acoustic emissions during butt welding by CW YAG laser. Proceedings of SPIE - The International Society for Optical Engineering 4831:148
23. Pordzik R, Mattulat T, Woizeschke P (2022) Effects of reduced ambient pressure on the OCT-based weld depth measurement signal in laser welding of aluminum and steel. Procedia CIRP 111:541–546